论著·神经科学

测序解析3种肥胖模型小鼠下丘脑神经通讯特征:抑制性调控减弱,谷氨酸、NO与电突触信号各显主导

周连宇[1],费兴杭[1],尹华春[1],臧振乐[1],郑 新[1],范晓棠[2],李 松[1],杨 辉[1] 陆军军医大学(第三军医大学):[1]第二附属医院神经外科,[2]心理系军事认知心理学教研室,重庆

[摘要] **目的** 对比高脂饮食(high-fat diet,HFD)、瘦素突变(ob/ob)、瘦素受体突变(db/db)3种不同肥胖模型小鼠下丘脑细胞构成以及神经通讯网络变化识别可跨病因验证的普适机制线索、寻找适用于病因分层的特异靶点。**方法** 实验对6周龄雄性C57小鼠给予高脂饮食连续喂养至18周龄,建立饮食诱导性肥胖(HFD)模型;同时选用18周龄雄性瘦素缺陷(ob/ob)和瘦素受体缺陷(db/db)遗传性肥胖小鼠,并以同龄雄性C57小鼠作为对照。每组取3只(n=3),共12只。处死后在体视显微镜下精细切取下丘脑组织。采用10x Genomics v3.1平台进行单细胞核转录组测序(snRNA-seq),数据经Cell Ranger比对后导入Seurat完成质控、降维与聚类分析;随后基于NeuronChat及其神经系统特异性配体-受体数据库推断神经元-神经元通讯网络,系统比较各肥胖模型与C57对照组在差异通讯网络、信号输出/输入强度、信息流及作用数量等方面的变化。**结果** 单细胞转录组测序对C57、HFD、ob/ob及db/db小鼠下丘脑细胞进行降维聚类后,识别出包括兴奋性神经元、抑制性神经元及多类非神经元细胞在内的主要细胞群,不同模型同类细胞在UMAP空间存在一定偏移。对神经元二次聚类得到7个GABA能与10个谷氨酸能亚群,提示下丘脑神经元具有显著异质性。3种模型均呈现出GABA能抑制性输入和神经黏附分子-神经连接蛋白(Nrxn- Nlgn)通路信号普遍下调的特征,且不同模型间存在差异性神经通讯网络:HFD模型以缝隙连接蛋白α-1(Gja1-Gja1)电突触增强、Nrxn-Nlgn输出减少为特征;db/db模型以一氧化氮-鸟苷酸环化酶1可溶性亚基alpha 2(NO-Gucy1a2)及强啡肽原(Pdyn)通路占优;ob/ob模型以谷氨酸受体互作增强为主。模型间两两比较进一步验证:HFD相对富集Gja1及部分代谢型谷氨酸受体互作,db/db相对富集NO-Gucy1a2及突触黏附相关通路,ob/ob相对富集离子型/代谢型谷氨酸受体互作。**结论** 不同病因的肥胖模型中,下丘脑存在不同的神经通讯网络模式:饮食性肥胖更突出电突触相关通路增强,瘦素受体缺失模型以NO相关信号增强为主要特征,瘦素缺失模型则以谷氨酸能兴奋性互作增强为核心改变。但抑制性调控减弱是共同环节,为理解肥胖发生的病理机制提供了新的启示。

[关键词] 肥胖模型;下丘脑;单细胞核测序;神经通讯;配体-受体互作

[中图法分类号] R589.2;R338.2;Q811.4 [文献标志码] A

[基金项目] 国家自然科学基金(32471027);重庆市科技创新与应用发展专项(CSTB2024TIAD-STX0044);重庆市自然科学基金(CSTB2024NSCQ-MSX0021)

[通信作者] 杨 辉,E-mail:Yanghui@tmmu.edu.cn

李 松,E-mail:Tmmuls@tmmu.edu.cn

2097-0927/Copyright © 2026,陆军军医大学(第三军医大学)。这篇开放获取文章遵循CC BY许可协议(https://creativecommons.org/licenses/by/4.0/)

引用格式:周连宇,费兴杭,尹华春,等. 测序解析3种肥胖模型小鼠下丘脑神经通讯特征:抑制性调控减弱,谷氨酸、NO与电突触信号各显主导[J]. 陆军军医大学学报,2026,48(06):687-700. DOI:10.16016/j.2097-0927.202512099.

Citation:ZHOU L Y,FEI X H,YIN H C,*et al*. Hypothalamic neural communication characteristics in 3 mouse models based on sequencing analysis:Attenuated inhibitory regulation with dominant roles of glutamate,NO,and electrical synapse signaling[J]. J Army Med Univ,2026,48(06):687-700. DOI:10.16016/j.2097-0927.202512099.

Hypothalamic neural communication characteristics in 3 mouse models based on sequencing analysis: Attenuated inhibitory regulation with dominant roles of glutamate, NO, and electrical synapse signaling

ZHOU Lianyu[1], FEI Xinghang[1], YIN Huachun[1], ZANG Zhenle[1], ZHENG Xin[1], FAN Xiaotang[2], LI Song[1], YANG Hui[1]
[1]Department of Neurosurgery, Second Affiliated Hospital; [2]Department of Military Cognitive Psychology, College of Medical Psychology, Army Medical University (Third Military Medical University), Chongqing, China

[**Abstract**] Objective To compare the hypothalamic cellular composition and neuron-neuron communication networks across 3 etiologically distinct mouse models of obesity, high-fat diet (HFD), leptin-deficient (ob/ob), and leptin receptor-deficient (db/db) so as to identify universal mechanistic clues that can be validated across etiologies and searching for etiology-specific targets applicable to stratified treatment. Methods Six-week-old male C57 mice were fed with HFD continuously until 18 weeks of age to establish a HFD model. In parallel, 18-week-old male ob/ob mice and db/db mice were subjected as genetic obesity models, and age-matched male C57 mice served as controls. Three mice were included per group (n=3), totaling 12 mice, were euthanized, and the hypothalamic tissues were meticulously dissected under a stereomicroscope. Single-nucleus transcriptome sequencing (snRNA-seq) was performed using the 10x Genomics v3.1 platform. The obtained sequencing data were aligned with Cell Ranger and processed in Seurat for quality control, dimensionality reduction, and clustering. Subsequently, neuron-neuron communication networks were inferred based on NeuronChat and its nervous system-specific ligand-receptor database, systematically comparing changes in differential communication networks, signal output/input strength, information flow, and interaction quantity between each obesity model and C57 controls. Results Dimensionality reduction and clustering of hypothalamic snRNA-seq data from C57, HFD, ob/ob, and db/db mice identified several major cell populations, including excitatory neurons, inhibitory neurons, and multiple non-neuronal cell types, with cells of the same type showing model-dependent shifts in uniform manifold approximation and projection (UMAP) space. Neuronal subclustering resolved 7 GABAergic and 10 glutamatergic subtypes, indicating pronounced neuronal heterogeneity in the hypothalamus. Across the 3 obese models, GABAergic inhibitory incoming signaling and the neurexin-neuroligin (Nrxn-Nlgn) pathway were broadly downregulated. Meanwhile, each model exhibited a distinct communication-network signature: the HFD model was characterized by enhanced electrical synapses mediated by gap junction protein alpha-1 (Gja1-Gja1) and reduced Nrxn-Nlgn output; the db/db model showed dominant nitric oxide-soluble guanylate cyclase signaling (NO-Gucy1a2) together with enrichment of prodynorphin (Pdyn)-related pathways; the ob/ob model was primarily marked by enhanced glutamate receptor interactions. Pairwise comparisons among models further validated these patterns: HFD relatively enriched Gja1-related signaling and certain metabotropic glutamate receptor interactions; db/db relatively enriched NO-Gucy1a2 and synaptic adhesion-related pathways; ob/ob relatively enriched in ionotropic/metabotropic glutamate receptor interactions. Conclusion Distinct neural communication network patterns exist in the hypothalamus across obesity models of different etiologies: diet-induced obesity preferentially exhibits enhanced electrical synapse-related pathways, leptin receptor-deficient model is primarily characterized by increased NO-related signaling, and the leptin-deficient model is centrally distinguished by enhanced glutamatergic excitatory interactions. Notably, attenuated inhibitory regulation emerges as a common feature across models, providing novel insights into understanding the pathological mechanisms underlying obesity development.

[**Key words**] obesity animal models; hypothalamus; single-nucleus RNA sequencing; neuronal communication; ligand-receptor interactions

Supported by the National Natural Science Foundation of China (32471027), the Special Project of Science and Technology Innovation and Application Development of Chongqing (CSTB2024TIAD-STX0044), and the Natural Science Foundation of Chongqing (CSTB2024NSCQ-MSX0021). Corresponding authors: YANG Hui, E-mail: Yanghui@tmmu.edu.cn; LI Song, E-mail: Tmmuls@tmmu.edu.cn

全球肥胖率呈上升趋势,严重威胁到人类公共健康,同时也增加了糖尿病、非酒精性脂肪肝病等代谢性疾病的发病几率[1]。肥胖的根本原因是机体内能量过剩,超出身体需求的能量会以三酰甘油的形式,贮存于皮下(SAT)或者内脏(VAT)的白色脂肪组织中,进而致使机体出现全身性的代谢异常[2]。ob/ob、db/db和HFD小鼠分别用于模拟瘦素通路缺陷以及"环境-基因"交互作用,能够重现肥胖从适应阶段至病变阶段的全过程。众所周知,下丘脑是能量代谢的中枢,其中弓状核(arcuate nucleus,ARC)、室旁核(paraventricular hypothalamus,PVH)、腹内侧核(ventromedial nucleus,VMH)协同发挥着重要作用[3-6]。已有文献报道,正常小鼠VMH区代谢型谷氨酸受体5型的表达受热量状态的调控,而在严重肥胖、葡萄糖平衡受损的BDNF突变鼠中,该受体的表达水平显著降低[7],当体重下降时,PVH^{TRH}至ARC^{AgRP}环路轴突数量的增加会促进食欲增加和体重反弹[8]。这些研究结果提示,突触结构与受体分布的稳定性以及神经通讯环路在能量稳态中的重要性。然而,目前肥胖患者下丘脑神经通讯环路尚不明确,这阻碍了精准治疗的开展。

单细胞核RNA测序(single-nucleus RNA sequencing)能够在单细胞尺度上解析神经元和胶质细胞的异质性[9-10]。在此基础上发展出众多新技术,这些技术可通过定量检测信号通路连接强度及信息传递方向,来理解复杂组织内的细胞网络互联关系[11-12]。其中,NeuronChat等具有神经系统特色的工具整合了神经递质、神经肽等配体-靶标的数据库,在细胞亚群层面能够推测并可视化神经元间的通讯网络[13]。这些新技术为从转录组水平上比较不同肥胖模型的神经通讯通路重塑轨迹提供了技术手段,并可在"细胞-配体-受体"层面上解析能量稳态异常的神经通讯状态[9,11]。

然而,目前对不同病因驱动的肥胖在下丘脑微环路层面的细胞-细胞通讯重塑是否存在差异,仍缺乏系统性的并列比较。既往研究多聚焦于单一模型、单一核团或少数候选通路,难以从网络层面解析肥胖中枢机制的异质性来源。因此,对不同肥胖模型的下丘脑通讯网络进行解析与对比,有助于识别可跨病因验证的普适机制线索、寻找适用于病因分层的特异靶点。

1 材料与方法

1.1 实验动物

6周龄雄性C57使用高脂饲料(XTHF60,60%脂肪,协同生物)及对照饲料(XTCON50J,协同生物)饲养至18周龄进行实验(HFD)。18周龄雄性瘦素(leptin)突变型ob/ob(C57BL/6JGpt-$Lep^{em1Cd25}$/Gpt,Strain NO. T001461,集萃药康)小鼠以及瘦素受体(leptinr)突变型db/db(BKS-$Lepr^{em2Cd479}$/Gpt,Strain NO. T002407,集萃药康)小鼠购自集萃药康公司,饲养于陆军军医大学实验动物中心。动物房控制在20~23 ℃,湿度60%~70%,每12小时昼夜循环(8:00-20:00)可以自由进食和饮水。实验过程中密切监测小鼠状态变化,若出现体质量持续下降超过20%、明显运动障碍或伤口严重感染等状况,立即启动人道终点,对小鼠实施安乐死。实验期间无预期外不良事件发生,所有小鼠完成预设实验流程。所有操作流程符合陆军军医大学实验动物伦理审查委员会审查标准,已获得陆军军医大学实验动物伦理委员会批准(AMUWEC20237516)。每组取3只小鼠进行测序,生物学重复均为3(n=3)。

1.2 方法

1.2.1 18周龄C57、HFD、ob/ob与db/db小鼠下丘脑组织显微取样 1%戊巴比妥钠(50 mg/kg,i.p.)麻醉后取脑,冰浴保存。参照小鼠脑立体定位图谱(Paxinos and Franklin,第四版),于体视显微镜(瑞沃德)下切取下丘脑组织。解剖边界如下:前后边界自前连合(Bregma+0.14 mm)至乳头体(Bregma -2.9 mm);腹侧边界为脑底面(包括视交叉及正中隆起);背侧边界以穹窿腹侧缘为标志;外侧边界沿视束内侧缘。切取的组织经PBS冲洗后液氮速冻,用于后续单细胞悬液制备。

1.2.2 单细胞核悬液制备、建库与测序及初步质控 冻存下丘脑冰浴转入预冷的细胞核分离缓冲液(10 mmol/L Tris-HCl pH 7.4、10 mmol/L NaCl、3 mmol/L $MgCl_2$、0.1% NP-40及蛋白酶抑制剂),冰浴匀浆,40 μm滤膜过滤的单细胞核悬液。单细胞文库构建采用10x Genomics v3.1平台,每份样本8 000~10 000个细胞。测序所得原始文件通过Cell Ranger(v6.1.2)进行比对并生成gene-barcode矩阵。数据导入Seurat(v4.3.0)中进行质控和标准化,过滤标准:nFeature_RNA 100-6 000、nCount_RNA<15 000、线粒体基因比例<10%。随后采用SCTransform进行归一化,并用FindVariableFeatures法提取高变基因2 000个,基于PCA使用前30个PC进行降维并进一步UMAP可视化。通过Louvain聚类得到各类细胞群,并结合典型Marker基因对细胞进行注释。进一步对GABAergic与Glutamatergic能神经元提取后重聚类获得GABA-1~7与GLU-1~10亚群,作为后续神经通讯分析的基础。

1.2.3 NeuronChat神经元互作解析 本研究基于单细胞核测序获得的下丘脑神经元亚群数据,采用

NeuronChat(v0.3.1)的神经系统特异的配体-受体数据库(NeuronChatDB.mouse)进行神经元-神经元通讯推断[13]。通信链接(communication links)的统计显著性由置换检验确定,并使用FDR校正(q<0.05),为提高稳定性,每个样本重复100次bootstrap估计信号强度并取平均。

1.2.3.1 通讯矩阵构建 对经过Seurat标准流程处理过的下丘脑神经元单细胞表达矩阵进行归一化(scale.factor=10 000)后,以高变基因为输入生成NeuronChat对象,将不同的组别细胞簇注释(GABA-1~7、GLU-1~10等)作为细胞类型的标签输入,通讯数据库选择NeuronChatDB.mouse。

配体与靶点丰度估计按照NeuronChat默认方法进行:对于小分子递质(Glu、GABA),使用AND-OR逻辑计算,即对同一功能模块基因取算术平均(OR),跨模块基因取几何平均(AND)。非小分子配体与受体使用平均表达量计算。所有丰度值仅使用该基因在至少25%细胞中表达的数据点进行估计。程序参数:sender=NULL,receiver=NULL,N=0,M=100,fdr=0.05,K=0.5,method=NULL,mean method=NULL,strict=1。

1.2.3.2 信号输出与信号输入变化分析 依托显著通讯矩阵,分别计算每个细胞亚群的发送强度和接收强度。发送强度为该细胞群向所有其他细胞群发生的显著通讯值总和,接收强度为其接收的通讯值总和。两指标均在NeuronChat中按默认参数计算,并对所有细胞类型进行Z-score标准化,以用于可视化比较。跨组比较(C57 vs HFD、C57 vs ob/ob、C57 vs db/db)使用NeuronChat提供的compareNeuronChat函数,计算差异矩阵,输出数值。在输出的通信强度矩阵中,仅保留显著链接,非显著链接的数值均设为零。采用配对Wilcoxon检验以确定两个数据集之间是否存在显著差异。同时,使用效应大小(effectsize)评估统计方法,容忍度阈值为tol=0.05,评估差异的实际重要性。统计显著性依旧采用P<0.05阈值。

1.2.3.3 上调/下调通讯网络比较 对于实验组中显著通讯条目中,分别统计其配体-靶点链路上的差异值。

Δ Communication=Strength (experiment group) − Strength(control group)

差异方向是区分上下调通讯网络的标准。差异在NeuronChat中以替换检验的默认P<0.05为阈值进行筛选,并且同时剔除通信强度小于0.01 (min.strength=0.01)的链路,使用netVisual-diffComparison绘制上下调网络拓扑图,其节点大小表示该亚群总输出/输入能力,边宽代表差异强度。

1.2.3.4 信息流与作用数量分析 确定了显著的配体-受体链路后,通过信息流及作用数量指标来判断每一个信号通路在整个网络中所占的地位,信息流使用每个配体靶点对在通讯矩阵中绝对的通量和来定义,用computeNetSig(type="informationflow")函数得到。所有信息流的值归一化可以用于各组间比较,使用所有的显著链路数来定义作用数量(number of interaction)并通过countNet(type="pair")计算数值。

在跨组比较中计算:

ΔFlow=InformationFlow (experiment group) − InformationFlow(control group)

ΔNum=NumInteractions (experiment group) − NumInteractions(control group)

为减少低表达基因对估计的影响,对配体与靶点基因的表达过滤阈值设为:min.pct=0.1,min.avg=0.01。

1.2.3.5 GSVA富集分析 使用msigdbr下载小鼠GO的生理过程(BP)途径,保留包含差异配子对的所有途径。使用GSVA计算GABA细胞在不同组别中的全局得分。

1.3 统计学分析

所有统计检验为双侧检验(two-tailed),显著性水平设定为P<0.05,除特别说明外均按此标准判定差异具有统计学意义。

2 结果

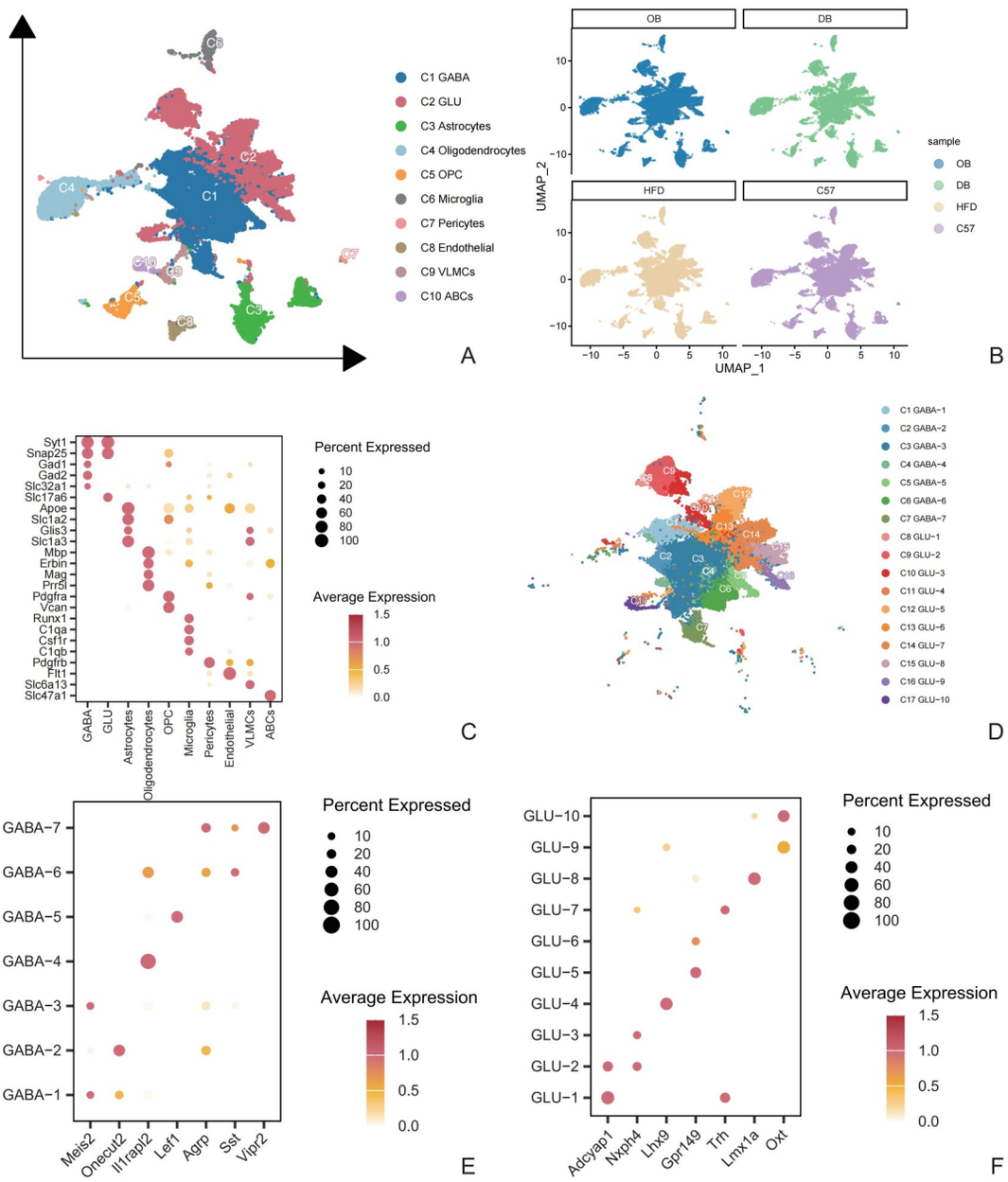
2.1 3种肥胖模型可引起下丘脑细胞转录状态偏移,并伴随GABA与谷氨酸能神经元亚群的重分布

对来自C57、HFD、ob/ob和db/db小鼠下丘脑的单细胞核测序结果进行降维与聚类(图1A),发现不同模型来源的同种类细胞呈现一定的空间偏移,提示疾病状态可能影响细胞转录特征。通过Findmarker并结合标记基因鉴定出主要的细胞类型,包括Gad1/2标记的γ氨基丁酸能神经元(GABAergic neuron)、Slc17a6标记的谷氨酸能神经元(glutamatergic neurons)、星形胶质细胞(astrocyte)、少突胶质细胞(oligodendrocyte)、少突胶质前体细胞(oligodendrocyte progenitor cells)、小胶质细胞(microglia)、周细胞(pericytes)、内皮细胞(endothelial cells)、血管软脑膜细胞(vascular leptomeningeal cells,VLMCs)等(图1B、C)。对神经元进行二次聚类后,其被细分为7个GABAergic亚群和10个glutamatergic亚群(图1D),提示下丘脑神经元具有高度异质性。随后,进一步给出了二次聚类后各GABA/GLU亚群的代表性标志基因,以及其可能对应

的神经元类型(图1E、F)。

2.2　不同肥胖模型导致下丘脑神经元间的抑制-兴奋平衡以模型特异的方式发生重塑

2.2.1　高脂饮食(HFD)诱导下丘脑GABA能抑制整



A: UMAP distribution of various cell types in the hypothalamus of C57, HFD, ob/ob, and db/db mice (n=3). Each point represents a single cell, with colors indicating major cell type clusters; B: UMAP distribution displayed by sample group (OB, DB, HFD, C57); C: Bubble plot showing the expression of marker genes for each cell type. Bubble size represents the proportion of cells expressing the gene (Percent expressed), and color indicates the average expression level (Average expression); D: UMAP showing neuronal subclusters, which are divided into multiple subgroups (GABA-1 to 7 and GLU-1 to 10); E: Bubble plot showing the expression of marker genes for GABAergic neuronal subclusters; F: Bubble plot showing the expression of marker genes for glutamatergic neuronal subclusters. UMAP: Uniform manifold approximation and projection; HFD: High-fat diet; ob/ob: Leptin-deficient mouse model; db/db: Leptin receptor-deficient mouse model; GABA: Gamma-aminobutyric acid; GLU: Glutamate

图1　下丘脑单细胞转录组图谱与亚群注释

Figure 1　Hypothalamic single-cell transcriptomic atlas and subtype annotation

体减弱,并伴随Gja1介导的缝隙连接与谷氨酸能信号增强　　HFD小鼠下丘脑细胞间通讯网络架构显示,在上调通讯网络中(图2A),GLU-9与GABA-6等神经元亚群表现出活跃的信号发送状态。相反,在下调网络中(图2B),抑制性与兴奋性神经元之间原有的连接被显著削弱。随后,基于差异信号强度分析发现,在信号输出层面(图2C),GLU-9和GLU-1成为极强的信号发送源,而GABA-2和GLU-4亚群的输出则呈现整体性抑制状态。同时,几乎所有细胞的突触黏附Nrxn1/2/3-Nlgn2通路信号输出显著减少。在信号接收层面(图2D),所有神经元中GABA能抑制性通路信号输入显著减少。配体-受体互作数量与信息流的相对权重分析也进一步证实该结果(图2E、F)。HFD组激活的配体-受体互作通路中,Gja1-Gja1(缝隙连接蛋白)通路位居首位,其次为Glu-Grm3及Glu-Grm5等兴奋性通路,提示电突触通讯与谷氨酸能信号出现异常激活。与信号接收结果一致的是,C57组激活的配体-受体互作通路主要集中在GABA能抑制性通路(GABA-Gabra5、GABA-Gabrb1、GABA-Gabra1)以及突触黏附通路(Nrxn1-Nlgn2、Nrxn3-Nlgn2),提示HFD组下丘脑GABA能抑制功能减弱。

2.2.2　瘦素受体缺陷导致下丘脑GABA能抑制减弱,进而触发NO-Gucy1a2信号的代偿性增强　　db/db小鼠下丘脑细胞间通讯网络架构显示,在上调通讯网络中(图3A),GLU-10及GLU-9信号发送状态活跃。而在下调通讯网络中(图3B),抑制性神经元与兴奋性神经元之间原有的通讯连接被显著削弱。基于差异信号强度的分析发现,在信号输出层面(图3C),GLU-9与GLU-10成为极强的信号发送源,而GLU-4与GABA-2亚群的输出则呈现整体抑制状态。在信号接收层面(图3D),所有神经元中GABA能抑制性通路信号输入显著减少。然而NO-Gucy1a2信号输入对所有神经元显著增加。配体-受体互作数量与信息流的相对权重分析进一步证实了上述变化(图3E、F)。在db/db组激活的配体-受体互作通路中,NO-Gucy1a2(一氧化氮信号)通路位居首位,其次为谷氨酸Glu-Grm4兴奋性通路及Pdyn-Oprn1(强啡肽-阿片受体)通路,提示血管-神经单元互作及阿片类信号的异常激活。与信号接收结果一致的是,C57组激活的配体-受体互作通路中主要集中在GABA能抑制性通路(GABA-Gabra5、GABA-Gabra4、GABA-Gabra1)以及突触黏附通路(Nrxn1-Nlgn1、Nrxn3-Nlgn1),提示db/db组下丘脑GABA能抑制功能减弱。

2.2.3　瘦素缺乏引起下丘脑GABA能抑制丧失,并导致谷氨酸能突触信号的广泛过度激活　　ob/ob突变肥胖模型小鼠下丘脑细胞间通讯网络架构显示,在上调通讯网络中(图4A),GLU-6、GLU-9与GABA-6等神经元亚群表现出活跃的信号发送状态。相反,在下调通讯网络中(图4B),抑制性神经元与兴奋性神经元之间原有的广泛通讯连接被显著削弱。基于差异信号强度的热图分析进一步揭示了具体的病理改变。在信号输出层面(图4C),GLU-9和GLU-10现为极强的信号发送源,成为优势输出源;而GLU-6与GABA-2亚群的输出则呈现整体性抑制状态。同时在几乎所有细胞中Nrxn1/2/3-Nlgn2通路信号输出显著减少。在信号接收层面(图4D),所有神经元中GABA能抑制性通路信号输入减少。配体-受体互作数量与信息流的相对权重分析进一步确证了上述变化(图4E、F)。ob/ob组激活的配体-受体互作通路中,Glu-Grm3与Glu-Grik4兴奋性通路强度占据绝对优势,Glu-Gria1(AMPA受体)也显著升高,提示谷氨酸能信号的全面过度激活。信号接收结果一致的是,C57组激活的配体-受体互作通路中主要集中在GABA能抑制性通路(GABA-Gabra5、GABA-Gabra1)以及突触黏附通路(Nrxn1/3-Nlgn1/2),提示ob/ob组下丘脑GABA能抑制功能减弱。

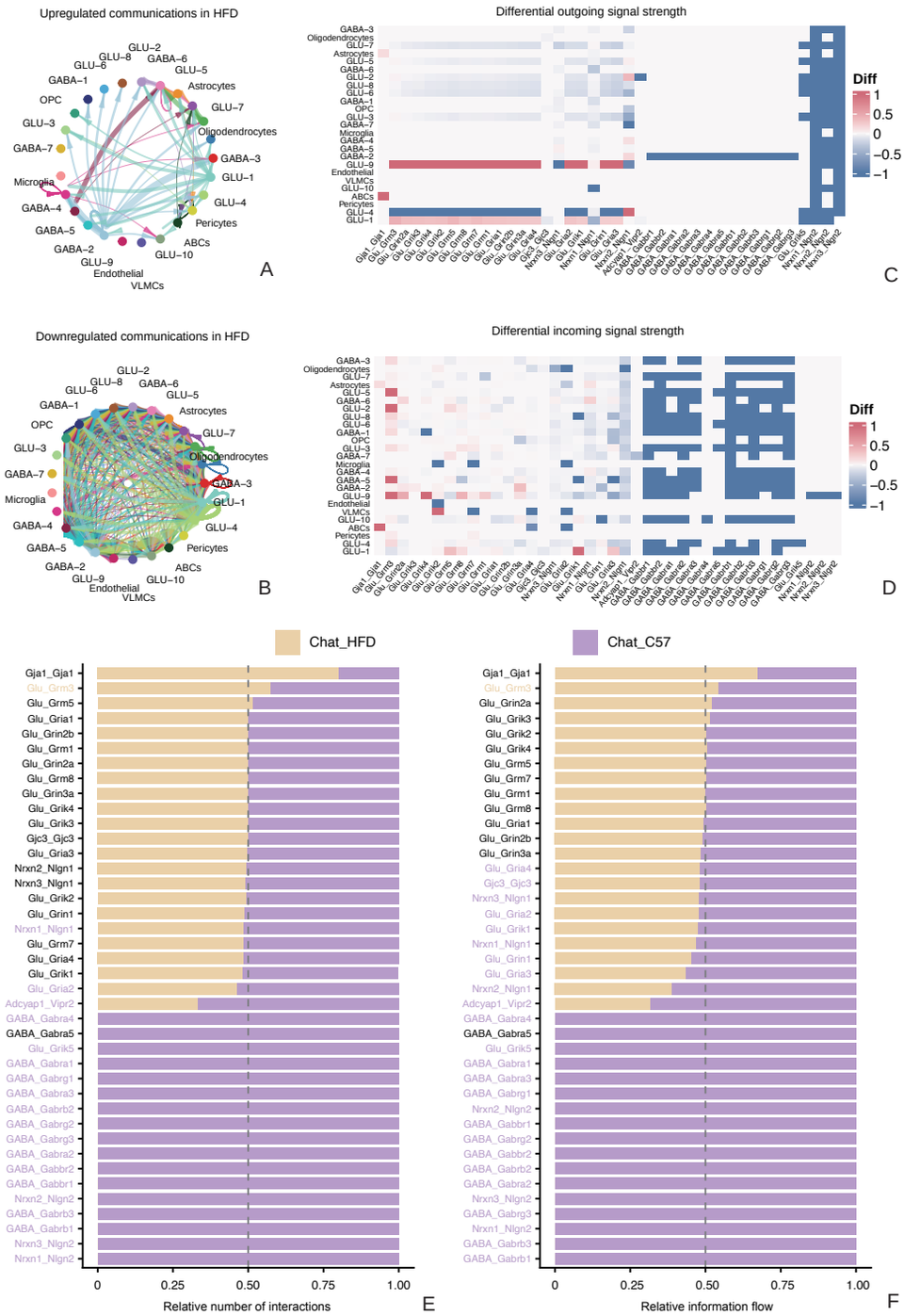
2.3　模型间直接比较揭示肥胖病因驱动的下丘脑神经通讯网络分型差异

为了进一步解析肥胖病因在神经网络重塑中的特异作用,进一步对3种肥胖模型进行了模型间两两比较。

ob/ob与db/db比较中(图5A~D),ob/ob以GLU-10与GLU-4为主要信号发送源,信息流由谷氨酸能兴奋性互作占据主导(Glu-Grik2、Glu-Grm3、Glu-Gria3),体现谷氨酸系统过度激活。ob/ob在与HFD比较中,ob/ob以GLU-4与GLU-1为强发送源,优势通路集中于离子型谷氨酸受体互作(Glu-Grin1、Glu-Grik4),并伴Nrxn-Nlgn突触黏附通路富集。

db/db与HFD比较(图5E~H),db/db侧GLU-10为显著增强的输出源,且神经元对NO-Gucy1a2通路的信号接收明显升高;通路权重主要聚焦于Nrxn1/2/3-Nlgn2突触黏附与NO-Gucy1a2以及Pdyn相关通路,提示突触结构连接及血管-神经互作/结构维持信号更占优势。db/db相较于ob/ob更倾向于富集NO-Gucy1a2、Trh-Trhr及Pdyn-Oprm1等血管-神经与激素/神经肽受体信号。

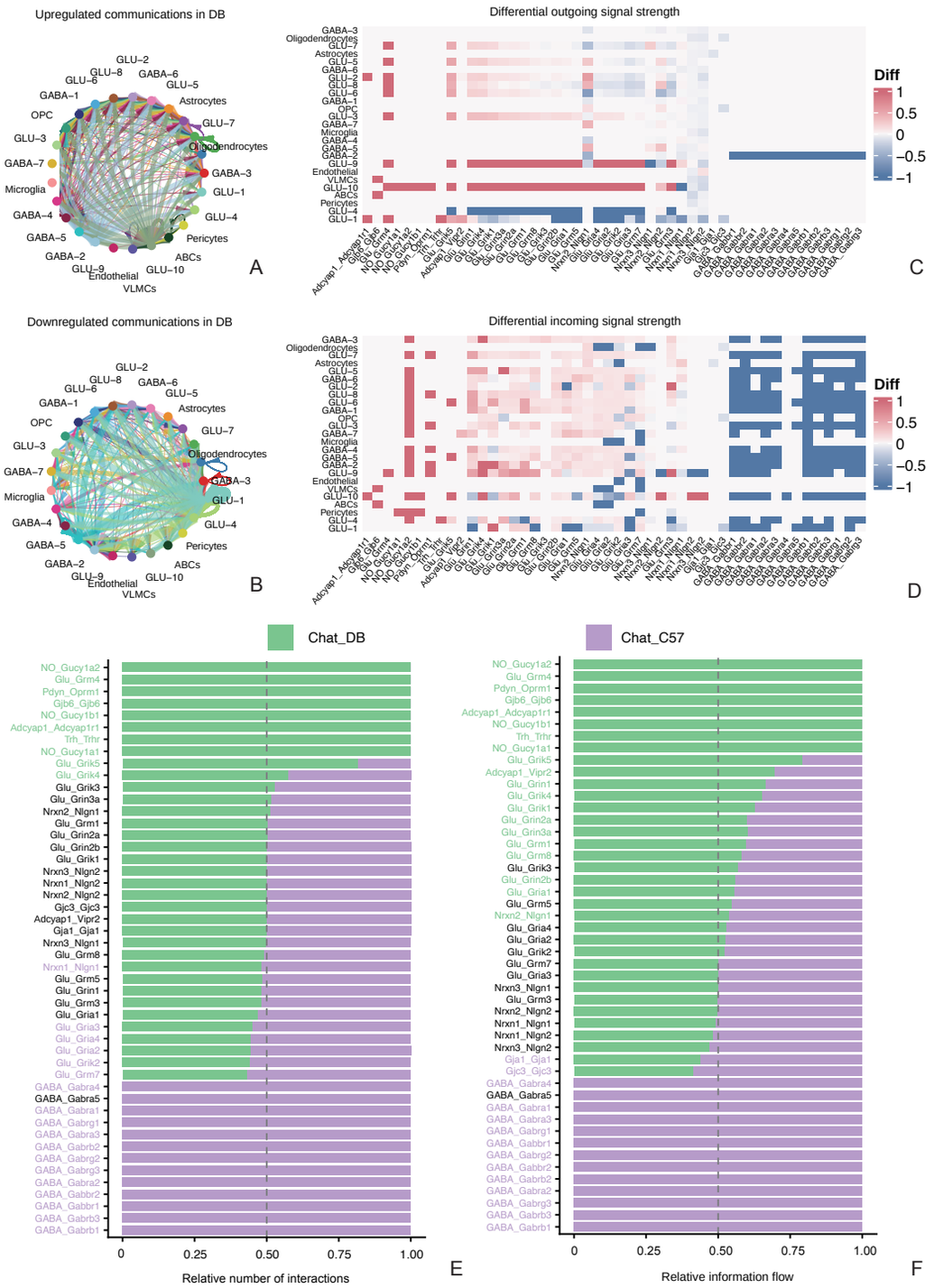
HFD相较于db/db表现出对Gja1及Glu-Grm信号接收的增加,优势通路集中于Gja1-Gja1缝隙连接与特定代谢型谷氨酸受体互作(Glu-Grm7/5/3),提示其跨



A and B: Significantly upregulated (A) and downregulated (B) ligand-receptor communication networks in the HFD group compared to the C57 control group. Lines in the network represent significant ligand-receptor interactions, and nodes represent cell types. Only communications that reached statistical significance *via* permutation testing (P<0.05) are shown; C and D: Heatmaps showing differential outgoing signaling (C) and incoming signaling (D) intensities. Red indicates enhanced signaling in the HFD group, while blue indicates enhanced signaling in the C57 group. Only significant signaling pathways/communications (P<0.05, permutation test) are included in the heatmaps; E: Bar graph comparing relative numbers of interactions. This shows the normalized proportion of significant communications within each signaling entry for the 2 groups; F: Bar graph comparing relative information flow. This shows the normalized proportion of total communication probability/weight for each signaling entry between the 2 groups. HFD: High-fat diet

图2 NeuronChat推断的HFD组与C57组之间的神经元通讯差异

Figure 2 NeuronChat-inferred neuronal communication differences between the HFD group and the C57 group

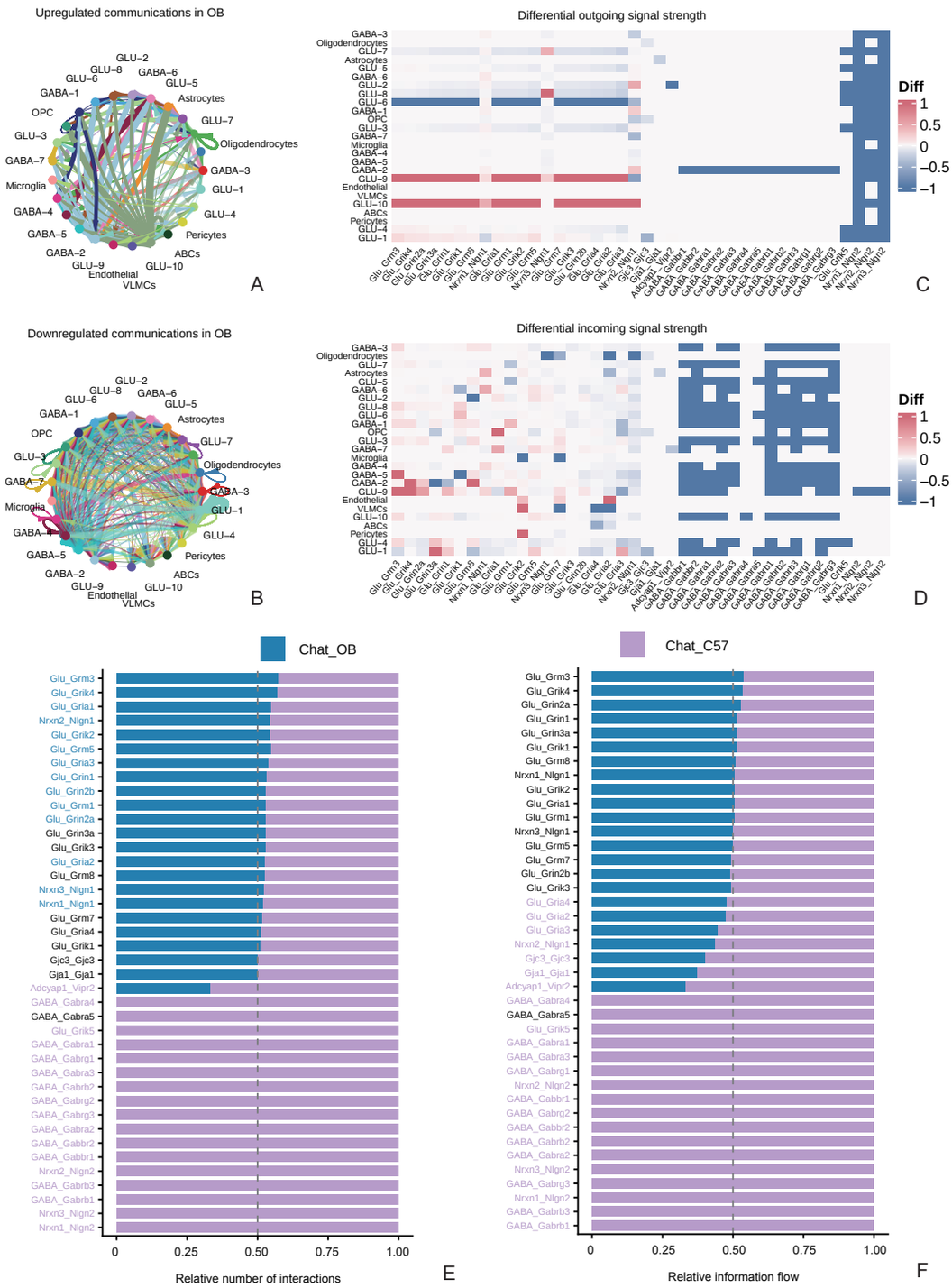


A and B: Significantly upregulated (A) and downregulated (B) ligand-receptor communication networks in the db/db group compared to the C57 control group; C and D: Heatmaps showing differential outgoing signaling (C) and incoming signaling (D) intensities; E: Bar graph comparing relative numbers of interactions; F: Bar graph comparing relative information flow. db/db: Leptin receptor-deficient mouse model

图3 NeuronChat推断的db/db组与C57组的神经通讯差异

Figure 3 NeuronChat-inferred neuronal communication differences between the db/db group and the C57 group

细胞电耦联与兴奋性输入负荷增加(图5I~L)。类似地,HFD与ob/ob比较中,HFD侧同样以Gja1-Gja1及Glu-Grm3/Grm1等代谢型谷氨酸通路为主要特征,表现为电突触通讯异常上调。

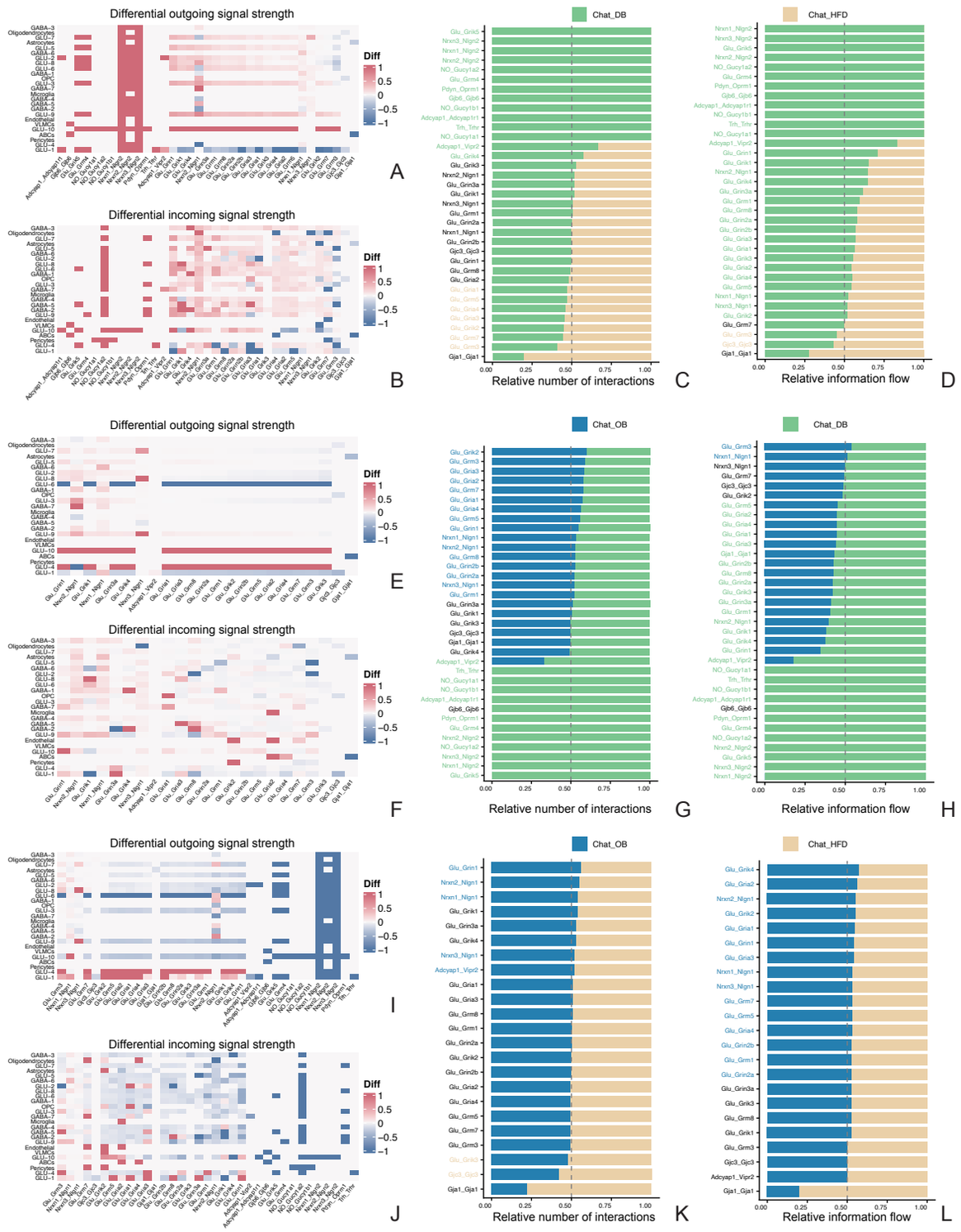


A and B: Significantly upregulated (A) and downregulated (B) ligand-receptor communication networks in the ob/ob group compared to the C57 control group; C and D: Heatmaps showing differential outgoing signaling (C) and incoming signaling (D) intensities; E: Bar graph comparing relative numbers of interactions; F: Bar graph comparing relative information flow. ob/ob: Leptin-deficient mouse model

图4 NeuronChat推断的ob/ob组与C57组的神经通讯差异

Figure 4 NeuronChat-inferred neuronal communication differences between the ob/ob group and the C57 group

同时,我们将3种肥胖模型小鼠共同出现的GABA配体-受体对所涉及的GO生物过程(BP)进行GSVA评分(图6)。结果显示,相较于C57组,对应于突触/神经递质传递与受体稳态的多项过程在肥胖组整体呈下降趋势,主要包括:神经递质分泌的正向调控(positive regulation of neurotransmitter secretion)、神



A, E, I: Heatmaps showing differential outgoing signaling intensities between the db/db and HFD groups (A), ob/ob and db/db groups (E), and ob/ob and HFD groups (I); B, F, J: Heatmaps showing differential incoming signaling intensities between the db/db and HFD groups (B), ob/ob and db/db groups (F), and ob/ob and HFD groups (J); C, G, K: Bar graphs comparing relative numbers of interactions between the db/db and HFD groups (C), ob/ob and db/db groups (G), and ob/ob and HFD groups (K); D, H, L: Bar graphs comparing relative information flow between the db/db and HFD groups (D), ob/ob and db/db groups (H), and ob/ob and HFD groups (L). HFD: High-fat diet; ob/ob: Leptin-deficient mouse model; db/db: Leptin receptor-deficient mouse model

图5 不同肥胖模型间神经元通讯的两两比较分析

Figure 5 Pairwise comparison analysis of neuronal communication across different obesity models

经递质运输的正向调控(positive regulation of neurotransmitter transport)和神经递质门控离子通道聚集(neurotransmitter-gated ion channel clustering)等。

3 讨论

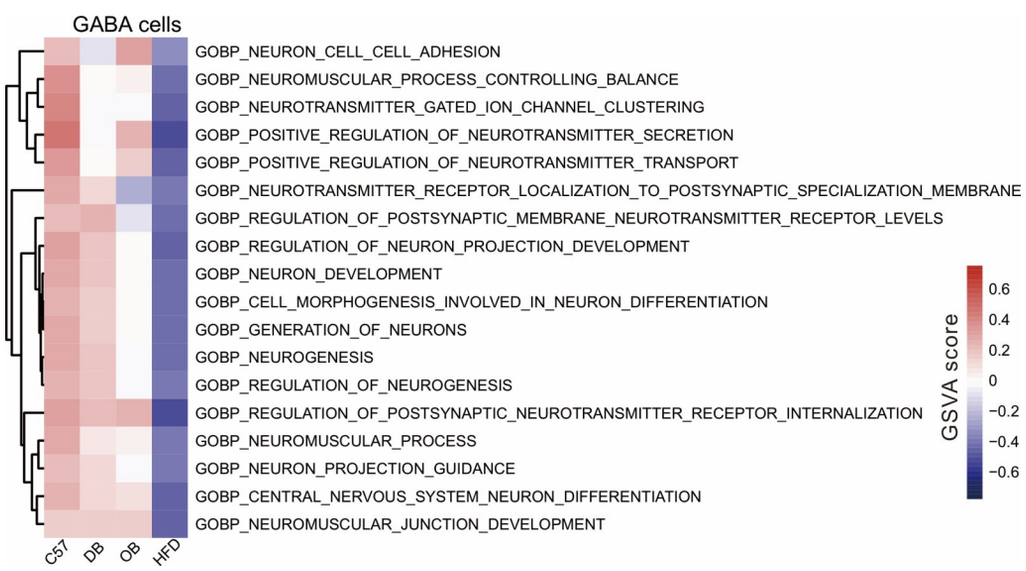
HFD、ob/ob和db/db均为研究中常用的肥胖模型,但存在不同的病因。既往研究报道HFD、ob/ob及db/db小鼠下丘脑弓状核-室旁核-外侧下丘脑(ARC-PVN-LH)微环路均表现出兴奋-抑制(E/I)失衡、胶质瘢痕化及POMC神经元突触丢失等共同病理特征[14-16]。本研究通过单细胞核测序分析,证实了不同肥胖模型中下丘脑区域存在着共同的抑制性神经通讯减弱,以及存在差异化的神经通讯网络变化,揭示了下丘脑神经环路在不同病因肥胖模型中的分子变化。

3.1 饮食性肥胖诱导的下丘脑神经通讯重塑以电突触相关信号增强为主要特征

HFD诱导下丘脑细胞通信重编程的特征在于电突触相关通路的激活,这提示饮食性代谢负担可能首先通过修饰细胞间快速同步和电耦合的信息传递来实现。既往研究表明,在代谢应激状态下,Gja1/Cx43的表达变化可能参与能量稳态的调控[17],而且Cx43通道激活有助于摄食调节相关信号分子的释放[18]。由此可见,HFD模型中电突触相关通路增强可能是由于Cx43相关功能异常导致的。然而,上述通路增强的结果是基于算法推断得出的,仍需通过电生理、示踪或者特异性阻断等方式证实HFD模型中电突触耦合和通道的功能作用[19-20]。本研究发现,HFD显著激活下丘脑电突触相关通路,表现为Gja1/Cx43表达上调及电突触功能增强。该结果与既往研究一致:弓状核伸长细胞(tanycyte)中Cx43缺失会破坏葡萄糖-乳酸代谢耦联,抑制POMC神经元活性,从而诱发贪食、体重及脂肪量增加并降低能量消耗[21]。在ARC和下丘脑/背侧迷走神经复合体区,胶质细胞Cx43与突触元件形成80%~85%空间共定位,提示其持续释放信号分子调控神经环路[22]。我们推测其异常可能与GABA能抑制性相关输入整体减弱有关。总的来说,HFD模型中电突触相关的重塑具有一定的特异性,这说明饮食诱导的肥胖和遗传性肥胖可能存在着不同的关键神经机制。

3.2 db/db瘦素受体缺失模型的下丘脑神经通讯改变与NO信号及神经血管互作相关

db/db模型中NO-Gucy1a2相关信号轴是通讯网络变化的关键所在。当瘦素受体缺失时,下丘脑局部的NO-sGC-cGMP通路可能被激活,并参与网络重塑。研究表明,NO信号在脑血管舒缩调节、局部灌注匹配及神经血管单元功能维持中具有明确作用[23-25],该通路



Heatmap showing the GSVA scores of significantly enriched GO-BP pathways in GABAergic neurons across different groups (C57, DB, OB, HFD) and their hierarchical clustering results. Color represents the GSVA score (red for upregulation, blue for downregulation; the intensity of the color reflects the magnitude of change). HFD: High-fat diet; ob/ob: Leptin-deficient mouse model; db/db: Leptin receptor-deficient mouse model

图6 GABA能神经元中GO生物过程(BP)的GSVA评分热图

Figure 6 GSVA score heatmap of GO biological processes (BP) in GABAergic neurons

的上调提示瘦素信号障碍会引起局部血供和代谢的变化。既往研究表明，一氧化氮(NO)作为中枢神经系统的重要细胞间调节因子参与能量稳态调控。非特异性抑制脑内一氧化氮合酶(NOS)可降低小鼠摄食量并减少体重，而特异性敲除下丘脑 $NOS1^{+}$LepRb 神经元则导致暴食性肥胖、能量消耗下降及高血糖，表型近似全身 LepRb 缺失，提示 NO/NOS1 信号是瘦素介导能量平衡调控的关键环节[26]。NO 可同时上调 PKG 和下调 PKA 来抑制视网膜 GABAA 受体的功能[27]，因此我们推测 db/db 中 NO-sGC(Gucy1a2)轴异常可能参与本研究观察到的 GABA 能抑制性相关输入总体减弱。然而，突触黏附相关通路在 db/db 模型中的变化相对有限，提示该模型对突触结构连接的影响可能具有一定选择性，并非进行全面性重塑，这也与此前有关瘦素受体异常导致认知异常表型的相关结论有所对应[28]。此外，pdyn-阿片受体配对也得到增强，表明神经肽系统在瘦素受体缺失情况下起到了代偿作用[29]。总之，db/db 模型通讯重构的重点是 NO 信号及相关通路，以及血管-神经互作路径强度的增强。

3.3 ob/ob 瘦素缺失模型的下丘脑神经通讯以谷氨酸能通路增强为核心变化

ob/ob 模型中，谷氨酸及其离子型和代谢型受体相关的配对均上调，提示瘦素缺失增加了对下丘脑兴奋性输入信号的调控，提高了环路活动兴奋性[30-31]。因此对于谷氨酸能通路持续增强的 ob/ob 模型来说，可能不仅会导致其摄食及能量平衡异常，对中枢神经系统稳定性也会造成影响[32]。进一步地，Glu-Grm3、Glu-Grik4 等代谢型与离子型谷氨酸受体相关配对的协同变化提示该过程可能同时涉及突触前释放、突触后受体响应等多个环节[33-34]。既往研究表明，ob/ob 小鼠补充瘦素可快速调控 ARC 神经元间的突触连接数量与类型(兴奋 vs 抑制)，重塑摄食神经环路以抑制食欲和维持能量稳态[35]。瘦素可通过 Jak2-PI3K 信号通路在突触前水平降低腹侧被盖区多巴胺神经元的谷氨酸释放概率，兴奋性突触强度的减弱被认为是瘦素抑制奖赏性进食行为的重要神经基础。此外，下丘脑尾侧弓状核富集的谷氨酸能神经元直接受瘦素兴奋、被促食肽抑制，并通过快速激活 POMC 神经元发挥厌食作用，确立其作为负向能量平衡调控的关键兴奋性节点[36-37]。上述结果提示 ob/ob 型肥胖的干预或可从谷氨酸能信号通路的调控入手。

3.4 不同病因肥胖模型共同呈现 GABA 能输入相关功能减弱

尽管 3 种肥胖模型的发病机制各异，但我们发现 3 种肥胖模型均存在 GABA 能抑制性输入降低这一共性变化。由此说明抑制性网络是发生代谢紊乱时较为统一且敏感的易损环节。同时，GABA 能抑制性输入下降会打破下丘脑局部兴奋和抑制之间的平衡，而肥胖相关的异常情绪、行为等精神躯体症状，可能是由兴奋和抑制失衡引起的[38-39]。除激素和神经肽调控外，突触传递及其可塑性同样决定下丘脑神经元的输出模式。能量过剩可通过重塑兴奋/抑制(E/I)平衡削弱中枢负反馈，导致摄食终止信号受损并驱动持续性进食。多项研究已证实，肥胖状态下 GABA 能抑制减弱在能量代谢失衡中发挥关键作用，高脂饮食可通过增强非突触 GABA 抑制或改变神经环路活动，降低能量消耗并促进体重增加，而恢复 GABA 能神经元活性则可显著改善肥胖表型[40-42]。另外，这 3 种模型的 GABA 能系统与突触黏附分子相关的变化均存在一定的相似性，其中 Nrxn-Nlgn 轴功能障碍提示细胞黏附分子参与调节突触结构稳定和功能维持[43-44]。因此，围绕 GABA 能输入和突触结构稳定性开展验证和干预，有望找到具有普适性的肥胖干预切入点。

总体而言，本研究从“细胞亚群-配体/靶点”互作层面，对饮食性与两类遗传性肥胖模型的下丘脑通讯重塑进行了比较，为理解肥胖状态下神经通讯失衡提供了系统的证据，也为未来在不同病因背景下制定干预策略提供了方向。在接下来的更多工作中，我们将围绕核心通路的蛋白表达与功能检测展开更多的基因功能富集分析，并将通讯变化与神经元亚群基因表达谱关联，以及实验验证。

利益冲突 本文所有作者声明不存在利益冲突

参考文献：

[1] 姚宇，候鹏飞，周敏，等. 吲哚-3-丙酸通过调节脂肪组织代谢改善高脂饮食诱导代谢相关脂肪性肝病的作用及机制研究[J]. 陆军军医大学学报，2024，46(9)：919-927. DOI:10.16016/j.2097-0927.202309045.
YAO Y，HOU P F，ZHOU M，*et al*. Role and mechanism of indole-3-propionic acid improving metabolic associated fatty liver disease by regulating adipose tissue metabolism[J]. J Army Med Univ，2024，46(9)：919-927. DOI:10.16016/j.2097-0927.202309045.

[2] QIAN S W，TANG Y，TANG Q Q. Adipose tissue plasticity and the pleiotropic roles of BMP signaling[J]. J Biol Chem，2021，296：100678. DOI:10.1016/j.jbc.2021.100678.

[3] XU B J，XIE X Y. Neurotrophic factor control of satiety and

body weight[J]. Nat Rev Neurosci, 2016, 17(5): 282-292. DOI:10.1038/nrn.2016.24.

[4] DE SOLIS A J, DEL RÍO-MARTÍN A, RADERMACHER J, *et al*. Reciprocal activity of AgRP and POMC neurons governs coordinated control of feeding and metabolism [J]. Nat Metab, 2024, 6(3): 473-493. DOI: 10.1038/s42255-024-00987-z.

[5] WANG A, SPEAKMAN J R. Potential downsides of calorie restriction[J]. Nat Rev Endocrinol, 2025, 21(7): 427-440. DOI:10.1038/s41574-025-01111-1.

[6] 刘凌琳, 张俊鸿, 熊玮. 小鼠的下丘脑室旁核向前包钦格复合体直接投射参与调控呼吸[J]. 陆军军医大学学报, 2024, 46(20): 2265-2275. DOI: 10.16016/j. 2097-0927. 202408088.
LIU L L, ZHANG J H, XIONG W. Paraventricular hypothalamic nucleus projects directly to the preB? tzinger complex and is involved in regulation of respiration in mice [J]. J Army Med Univ, 2024, 46(20): 2265-2275. DOI: 10.16016/j.2097-0927.202408088.

[7] FAGAN M P, AMEROSO D, MENG A, *et al*. Essential and sex-specific effects of mGluR5 in ventromedial hypothalamus regulating estrogen signaling and glucose balance [J]. Proc Natl Acad Sci USA, 2020, 117(32): 19566-19577. DOI: 10.1073/pnas.2011228117.

[8] GRZELKA K, WILHELMS H, DODT S, *et al*. A synaptic amplifier of hunger for regaining body weight in the hypothalamus [J]. Cell Metab, 2023, 35(5): 770-785. e5. DOI:10.1016/j.cmet.2023.03.002.

[9] CHEN R C, WU X J, JIANG L, *et al*. Single-cell RNA-seq reveals hypothalamic cell diversity [J]. Cell Rep, 2017, 18(13): 3227-3241. DOI:10.1016/j.celrep.2017.03.004.

[10] DENG G R, MORSELLI L L, WAGNER V A, *et al*. Single-nucleus RNA sequencing of the hypothalamic arcuate nucleus of C57BL/6J mice after prolonged diet-induced obesity [J]. Hypertension, 2020, 76(2): 589-597. DOI: 10.1161/HYPERTENSIONAHA.120.15137.

[11] SHAO X, LU X, LIAO J, *et al*. New avenues for systematically inferring cell-cell communication: through single-cell transcriptomics data [J]. Protein Cell, 2020, 11(12): 866-880. DOI:10.1007/s13238-020-00727-5.

[12] CESARO G, NAGAI J S, GNOATO N, *et al*. Advances and challenges in cell-cell communication inference: a comprehensive review of tools, resources, and future directions [J]. Brief Bioinform, 2025, 26(3): bbaf280. DOI:10.1093/bib/bbaf280.

[13] ZHAO W, JOHNSTON K G, REN H, *et al*. Inferring neuron-neuron communications from single-cell transcriptomics through NeuronChat [J]. Nat Commun, 2023,14(1): 1128. DOI:10.1038/s41467-023-36800-w.

[14] THALER J P, YI C X, SCHUR E A, *et al*. Obesity is associated with hypothalamic injury in rodents and humans [J]. J Clin Invest, 2012, 122(1): 153-162. DOI:10.1172/JCI59660.

[15] BAVER S B, HOPE K, GUYOT S, *et al*. Leptin modulates the intrinsic excitability of AgRP/NPY neurons in the arcuate nucleus of the hypothalamus[J]. J Neurosci, 2014, 34(16): 5486-5496. DOI: 10.1523/JNEUROSCI. 4861-12.2014.

[16] VONG L, YE C, YANG Z F, *et al*. Leptin action on GABAergic neurons prevents obesity and reduces inhibitory tone to POMC neurons[J]. Neuron, 2011, 71(1): 142-154. DOI:10.1016/j.neuron.2011.05.028.

[17] DE SOUZA G O, CHAVES F M, SILVA J N, *et al*. Gap junctions regulate the activity of AgRP neurons and diet-induced obesity in male mice[J]. J Endocrinol, 2022, 255(2): 75-90. DOI:10.1530/JOE-22-0012.

[18] CHEN X, FANG X, ZHOU H, *et al*. Regulation of food intake by Connexin43 *via* adipocyte-sensory neuron electrical synapses [J]. Mol Metab, 2025, 101: 102247. DOI:10.1016/j.molmet.2025.102247.

[19] LI Y, FANG Y, LI K, *et al*. Morphological tracing and functional identification of monosynaptic connections in the brain: a comprehensive guide[J]. Neurosci Bull, 2024, 40(9): 1364-1378. DOI:10.1007/s12264-024-01196-0.

[20] SHEFFIELD M E J, ADOFF M D, DOMBECK D A. Increased prevalence of calcium transients across the dendritic *Arbor* during place field formation [J]. Neuron, 2017, 96(2): 490-504. e5. DOI: 10.1016/j. neuron. 2017. 09.029.

[21] LHOMME T, CLASADONTE J, IMBERNON M, *et al*. Tanycytic networks mediate energy balance by feeding lactate to glucose-insensitive POMC neurons [J]. J Clin Invest, 2021, 131(18): e140521. DOI:10.1172/JCI140521.

[22] GUILLEBAUD F, BARBOT M, BARBOUCHE R, *et al*. Blockade of glial connexin 43 hemichannels reduces food intake [J]. Cells, 2020, 9(11): 2387. DOI: 10.3390/cells9112387.

[23] DAI C, TAN M, MENG X P, *et al*. Effects of potassium channel knockdown on peripheral blood T lymphocytes and NFAT signaling pathway in Xinjiang Kazak patients with hypertension [J]. Clin Exp Hypertens, 2023, 45(1): 2169449. DOI:10.1080/10641963.2023.2169449.

[24] CARLSTRÖM M, WEITZBERG E, & LUNDBERG J O. Nitric oxide signaling and regulation in the cardiovascular system: recent advances[J]. Pharmacol Rev, 2024,76(6): 1038-1062. DOI:10.1124/pharmrev.124.001060.

[25] FABER J E. Collateral blood vessels in stroke and ischemic disease: Formation, physiology, rarefaction, remodeling [J]. J Cereb Blood Flow Metab, 2025, 45(6): 0271678X251322378. DOI:10.1177/0271678X251322378.

[26] MORLEY J E, FLOOD J F. Evidence that nitric oxide modulates food intake in mice[J]. Life Sci, 1991, 49(10): 707-711. DOI:10.1016/0024-3205(91)90102-h.

[27] WEXLER E M, STANTON P K, NAWY S. Nitric oxide depresses GABAA receptor function *via* coactivation of cGMP-dependent kinase and phosphodiesterase [J]. J Neurosci, 1998, 18 (7): 2342-2349. DOI: 10.1523/JNEUROSCI.18-07-02342.1998.

[28] FERNANDES C, FORNY-GERMANO L, ANDRADE M M, *et al*. Leptin receptor reactivation restores brain function in early-life Lepr-deficient mice[J]. Brain, 2024, 147(8): 2706-2717. DOI:10.1093/brain/awae127.

[29] OSAKADA T, YAN R Z, JIANG Y W, *et al*. A dedicated hypothalamic oxytocin circuit controls aversive social learning[J]. Nature, 2024, 626(7998): 347-356. DOI: 10.1038/s41586-023-06958-w.

[30] LIU Q, YANG X, LUO M, *et al*. An iterative neural processing sequence orchestrates feeding [J]. Neuron, 2023, 111 (10): 1651-1665. e5. DOI: 10.1016/j. neuron. 2023. 02.025.

[31] PETERSEN J, LUDWIG M Q, JUOZAITYTE V, *et al*. GLP-1-directed NMDA receptor antagonism for obesity treatment[J]. Nature, 2024, 629(8014): 1133-1141. DOI: 10.1038/s41586-024-07419-8.

[32] WANG F D, SUN H, CHEN M Y, *et al*. The thalamic reticular nucleus orchestrates social memory [J]. Neuron, 2024, 112 (14): 2368-2385. e11. DOI: 10.1016/j. neuron.2024.04.013.

[33] MUNGUBA H, SRIVASTAVA I, GUTZEIT V A, *et al*. Projection-targeted photopharmacology reveals distinct anxiolytic roles for presynaptic mGluR2 in prefrontal- and *Insula*-amygdala synapses[J]. Neuron, 2025, 113(6): 912-930.e6. DOI:10.1016/j.neuron.2025.01.002.

[34] LIOUTA K, LUBAS M, VENUGOPAL V, *et al*. LRRTM2 controls presynapse nano-organization and AMPA receptor sub-positioning through Neurexin-binding interface[J]. Nat Commun, 2024, 15(1): 8807. DOI:10.1038/s41467-024-53090-y.

[35] PINTO S, ROSEBERRY A G, LIU H Y, *et al*. Rapid rewiring of arcuate nucleus feeding circuits by leptin [J]. Science, 2004, 304 (5667): 110-115. DOI: 10.1126/science.1089459.

[36] THOMPSON J L, BORGLAND S L. Presynaptic leptin action suppresses excitatory synaptic transmission onto ventral tegmental area dopamine neurons [J]. Biol Psychiatry, 2013, 73 (9): 860-868. DOI: 10.1016/j.biopsych.2012.10.026.

[37] VAN DEN POL A N, ACUNA C, DAVIS J N, *et al*. Defining the caudal hypothalamic arcuate nucleus with a focus on anorexic excitatory neurons[J]. J Physiol, 2019, 597(6): 1605-1625. DOI:10.1113/JP277152.

[38] XIA G B, HAN Y, MENG F T, *et al*. Reciprocal control of obesity and anxiety-depressive disorder *via* a GABA and serotonin neural circuit[J]. Mol Psychiatry, 2021, 26(7): 2837-2853. DOI:10.1038/s41380-021-01053-w.

[39] XIE X Y, YANG H L, AN J J, *et al*. Activation of anxiogenic circuits instigates resistance to diet-induced obesity *via* increased energy expenditure [J]. Cell Metab, 2019, 29 (4): 917-931. e4. DOI: 10.1016/j. cmet. 2018. 12.018.

[40] PORNIECE M, BAKER J, AUSFAHL C D, *et al*. Obesity dysregulates feeding-evoked response dynamics in hypothalamic satiety neurons [J]. Sci Rep, 2025, 15: 35837. DOI:10.1038/s41598-025-19800-2.

[41] SA M, YOO E S, KOH W, *et al*. Hypothalamic GABRA5-positive neurons control obesity *via* astrocytic GABA[J]. Nat Metab, 2023, 5 (9): 1506-1525. DOI: 10.1038/s42255-023-00877-w.

[42] LI W, HUANG X, XU X, *et al*. Bright light exposure suppresses feeding and weight gain *via* a visual circuit linked to the lateral hypothalamus[J]. Nat Neurosci, 2025. DOI:10.1038/s41593-025-02156-1.

[43] SUN H Y, SHEN Y, NI P T, *et al*. Autism-associated neuroligin 3 deficiency in medial septum causes social deficits and sleep loss in mice[J]. J Clin Invest, 2024, 134 (19): e176770. DOI:10.1172/JCI176770.

[44] FRANKEL E B, TIROUMALECHETTY A, SU Z, *et al*. Intracellular protein-lipid interactions drive presynaptic assembly prior to neurexin recruitment [J]. Neuron, 2025, 113(5): 737-753.

(收稿:2025-12-18;修回:2026-01-25)

(编辑 严 涵)